Cooperative evolution of intraband and interband excitations for high-harmonic generation in strained MoS_2

Meng-Xue Guan,[1,2] Chao Lian,[1] Shi-Qi Hu,[1,2] Hang Liu,[1,2] Sheng-Jie Zhang,[1,2] Jin Zhang,[1,2] and Sheng Meng[1,2,3,*]

[1]*Beijing National Laboratory for Condensed Matter Physics and Institute of Physics, Chinese Academy of Sciences, Beijing 100190, China*

[2]*School of Physical Sciences, University of Chinese Academy of Sciences, Beijing 100190, China*

[3]*Songshan Lake Materials Laboratory, Dongguan, Guangdong 523808, China*

(Received 14 December 2018; revised manuscript received 13 May 2019; published 31 May 2019)

Modulating electronic structure of two-dimensional materials represents an exciting avenue for tailoring their optoelectronic properties. Here, we identify a strain-induced, cooperative effect of intraband and interband excitations contributing to high-harmonic generation (HHG) in prototype dichalcogenide MoS_2 monolayer. We find that besides the dominant intraband contributions, interband current is also indispensable in modulating HHG. The HHG yields increase linearly with the compressive strain since flatter band dispersion and Berry curvature enhance both interband and intraband dynamics. Band structure can be retrieved with high reliability by monitoring the strain-induced evolution of HHG spectra, suggesting that strain not only provides an additional knob to control HHG in solids, but also marks a way towards a complete understanding of underlying microscopic mechanisms.

DOI: 10.1103/PhysRevB.99.184306

I. INTRODUCTION

High-harmonic generation (HHG) in solids is a new frontier in attosecond science and materials physics, which has been observed in various condensed-matter systems [1–8]. It not only provides an alternative route for generating brighter and more compact attosecond pulses [6], but also enables potential access to multipetahertz electronics [9] and signal processing [10]. Meanwhile, HHG process stores information for reconstructing electronic band structure and Berry curvature, affording new opportunities for studying strong field and ultrafast electron dynamics in condensed phases [11–16]. Due to their diverse electronic structures, the interactions of solids with an ultrafast, intense pulse cannot be simply described by the three-step model developed for atomic gases [17–21]. Instead, two distinct processes, i.e., intraband and interband transitions, are believed to play decisive roles for solid-state HHG. The complex interplay between them can be controlled and utilized to improve the harmonic emission [22,23]. However, how the coupling between the two mechanisms influences the HHG yields is not obvious and is highly debated because they are nontrivially coupled and the relationship between them can be either competitive or cooperative [24,25]. The relative contributions of intraband and interband processes and total excitations may vary in different materials and spectral ranges, leading to large differences among various experimental observations. For instance, Wang *et al.* demonstrated that the dominant generation mechanism in ZnO would switch from interband to intraband transitions as the driving wavelength increases [26]. Therefore, it is highly desirable to identify the explicit roles of intraband and interband dynamics as well as the general trends in a realistic setting.

In addition to optical modulation methods, such as tuning polarization direction of laser field [27] and ellipticity [28,29], solid targets provide possibilities to control HHG via tailoring their electronic structure, either by chemical or structural engineering [4,5,30,31]. It is not only a means to actively manipulate the generation process, but also an analytical tool to study the properties of a given system. In a variety of solid-state materials, the ability to continuously tune material properties is one of the most unique features of two-dimensional crystals. Their electronic and optical properties are highly sensitive to external perturbations due to their atomic thickness [32]. In particular, monolayer transition-metal dichalcogenides (TMDs) such as MoS_2 have excellent mechanical properties that can withstand very large deformation before rupture, triggering a great interest in applying strain to tailor the crystal structure and modify their optoelectronic properties [33–36]. The effects of uniaxial compressive [37] or tensile strain [38] on the band structure of TMDs have been extensively studied by photoluminescence [39], Raman spectroscopy [40], and density-functional theory (DFT) [41,42]. Thus, it is reasonable to expect that strain will serve as an effective tool to control HHG in TMDs that, to date, remains unexplored.

In this work, using a full *ab initio* approach based on real-time time-dependent density-functional theory (RT-TDDFT) [19,43–47], we demonstrate high sensitivity of HHG to atomic-scale structural deformation by applying uniaxial strain in monolayer MoS_2. To gain insight into electron dynamics underlying harmonic emission, we performed both semiclassical analysis and quantum-mechanical dynamic simulations, showing that the HHG yield is sensitive and linearly dependent on strain, attributing to the fact that flatter band dispersion and Berry curvature help increase both intraband

*smeng@iphy.ac.cn

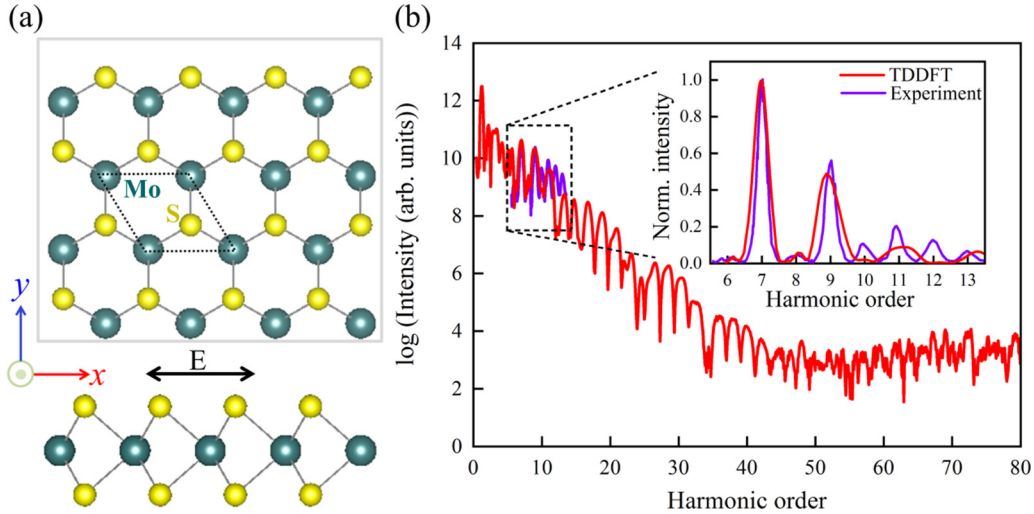

FIG. 1. (a) Schematic illustration of strained 1L-MoS_2 irradiated by linearly polarized laser pulse. The x, y axes are along the zigzag and armchair directions, respectively. (b) Computed HHG spectrum generated from primitive 1L-MoS_2 with the laser propagating along the zigzag direction (x). The inset shows the comparison between computed yields of the 6th to 13th harmonics (red) and the experimentally observed spectrum (purple) taken from Ref. [7]. The intensity of the seventh-order harmonic has been normalized to unity for both the calculated and experimental data.

and interband contributions. The two contributions display an interesting cooperative effect with strain, with the predominant contribution by the intraband current. Meanwhile, we propose a way to reconstruct the target band structure by monitoring the strain-dependent HHG spectra. This work provides a major step towards tuning HHG characteristics of a solid target via mechanical strain engineering.

II. THEORETICAL MODEL

A single layer of MoS_2 (1L-MoS_2) is a direct-gap semiconductor with an energy gap (E_g) of 1.8 eV, located at the valleys K and K' connected by time-reversible symmetry [48]. Comparing with its bulk counterpart and, thanks to the enhanced electron-hole Coulomb interactions [49–51] and inversion symmetry breaking [52,53], 1L-MoS_2 exhibits improved HHG efficiency and the emergence of even harmonics, making it distinctive for HHG emission.

The calculations are performed using the time-dependent *ab initio* package (TDAP) as implemented in SIESTA, which has been successfully developed to describe strong-field phenomena in solids [43–45]. Numerical atomic orbitals with double-zeta polarization (DZP) are employed as the basis set. The Brillouin zone is sampled by $36 \times 36 \times 1$ Gamma-centered $\boldsymbol{k}$ mesh with an energy cutoff of 250 Ry. The electron-nuclear interactions are described by Troullier-Martins pseudopotentials, in the adiabatic local-density approximation. It is important to note that within LDA, the band gap of semiconductor is underestimated and does not account for the excitonic effect. However, as the excitonic binding energy in TMDs is expected to be nearly independent of the uniaxial strain [54], thus relative variations in the electronic properties under strain and the resultant HHG spectrum are credible.

We consider both compressive and tensile uniaxial strain applied to the 1L-MoS_2 along, for example, the zigzag direction [Fig. 1(a)]. The results for other directions are qualitatively the same in our calculations (see Supplemental Material [55] for details). The strain is defined as $\varepsilon = \frac{a-a_0}{a_0}$, where a_0 and a are the equilibrium and strained lattice constants, respectively. As a result, compressive strain will induce direct-to-indirect gap transition at $\varepsilon \approx -1\%$ and increase the band gap, whereas a tensile strain ($\varepsilon > 0$) only slightly reduces the energy gap [Fig. S1(c)], in good agreement with experiments and previous calculations [42,56,57]. To study the HHG response of strained 1L-MoS_2, we adopt a linearly polarized laser beam with time-dependent electric field $E(t) = E_0 \cos(\omega t)\exp[-(t-t_0)^2/2\sigma^2]$. Velocity gauge is used where the vector and scalar potential of the field $E(t)$ are $\vec{A}(t) = -c\int_0^t \vec{E}(t')dt'$ and $\Phi = 0$. The photon energy and intensity are set as 0.32 eV and 2.24×10^{10} W/cm^2, respectively. The time evolution of the wave functions are then computed by propagating the Kohn-Sham equations in a.u.,

$$i\frac{\partial}{\partial t}\psi_i(\vec{r},t) = \left[\frac{1}{2m}\left(\vec{p} - \frac{e}{c}\vec{A}\right)^2 + V(\vec{r},t)\right]\psi_i(\vec{r},t), \qquad (1)$$

where the vector potential $\vec{A}(t)$ appears in the kinetic term. Then, time-dependent current can be obtained as

$$J(t) = \frac{1}{2i}\int_\Omega d\vec{r}\sum_i \{\psi_i^*(\vec{r},t)\nabla\psi_i(\vec{r},t) - \psi_i(\vec{r},t)\nabla\psi_i^*(\vec{r},t)\}. \qquad (2)$$

The HHG spectrum is obtained from time-dependent current through a Fourier transform,

$$\mathrm{HHG}(\omega) = \left|\int_0^T \omega^2 J(t)\exp(-i\omega t)dt\right|^2. \qquad (3)$$

The applied laser waveform and induced current are shown in Fig. 2.

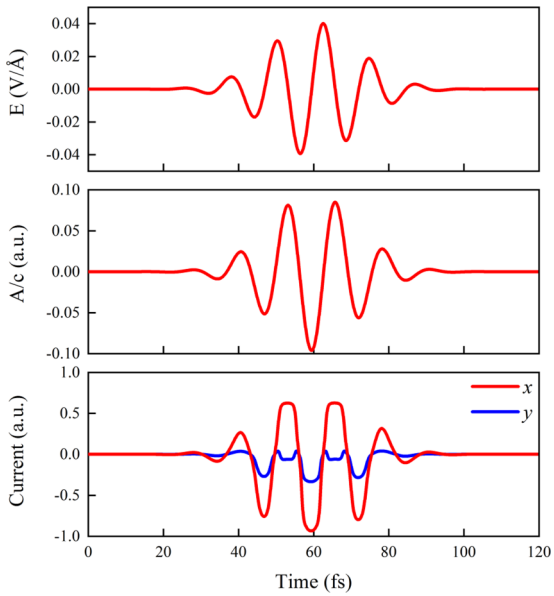

FIG. 2. Applied electric field (top), vector potential (middle), and induced electronic currents (bottom) that are parallel (red) or perpendicular (blue) to the incident polarization when $\varepsilon = 0$. The fundamental field centered at a photon energy of 0.32 eV and polarization direction along the zigzag (x) direction. We sum the total current from different directions and then the HHG spectrum $I(\omega)$ is shown in Fig. 1(b).

III. RESULTS AND DISCUSSION

To show the reliability of our theoretical approach, comparison between the calculated HHG spectrum and available experimental data [7] for strainless 1L-MoS_2 is shown in Fig. 1(b). The photon energy is set as one-sixth of the band gap of the primitive structure in both cases. Due to the low efficiency for higher-order responses, only the 6th to 13th harmonics are displayed in Ref. [7], where even-order emission is much weaker than the odd ones. The main features in experiment are well reproduced by our first-principles calculations, justifying the reliability of the present approach. We note that the differences between the two spectra can be ascribed to two reasons. One is that the laser polarization direction in our simulation might be different from the experiment (Fig. S2); the other potential reason is that neither dephasing nor propagation effects are considered in our simulations [55].

In order to investigate the role of structural deformation, HHG yield is monitored as a function of strain, shown in Fig. 3(a). The calculated spectra demonstrate the sensitivity of harmonic emission to small variations in the atomic structure. HHG yields for all orders increase by ∼10 to ∼150% when the lattice constant only changes by 3% under a compressive strain ($\varepsilon < 0$). However, for a tensile strain, enlarged strain reduces the HHG intensity at a lower rate. The above results indicate that the HHG yields can be continuously tuned by strain, and the compressive strain is more sensitive than tensile strain.

Figure 3(b) shows that the relative change in HHG intensity, i.e., $\frac{I_\varepsilon}{I_0}$ (I_ε and I_0 stand for the HHG yields with and without strain, respectively) is nearly linearly dependent on strain. However, the slopes of the fitted lines in Fig. 3(b) vary with the harmonic orders, i.e., the yields change at different rates. For each harmonic, we performed analysis on the corresponding absolute value of slope [Fig. 3(c)]. We notice that the slopes of even harmonics are generally larger than the odd ones, implying the different origins of the two kinds of harmonics. A semiclassical model based on acceleration theorem [58] was used to interpret the distinct polarization properties of odd and even harmonics in 1L-MoS_2 [7]. The validity of the model requires the absence of the interband tunneling and scattering processes. In other words, the adiabatic approximation implies that intraband transitions make the dominant contribution to emission, where the carriers are accelerated within the single band driven by laser field.

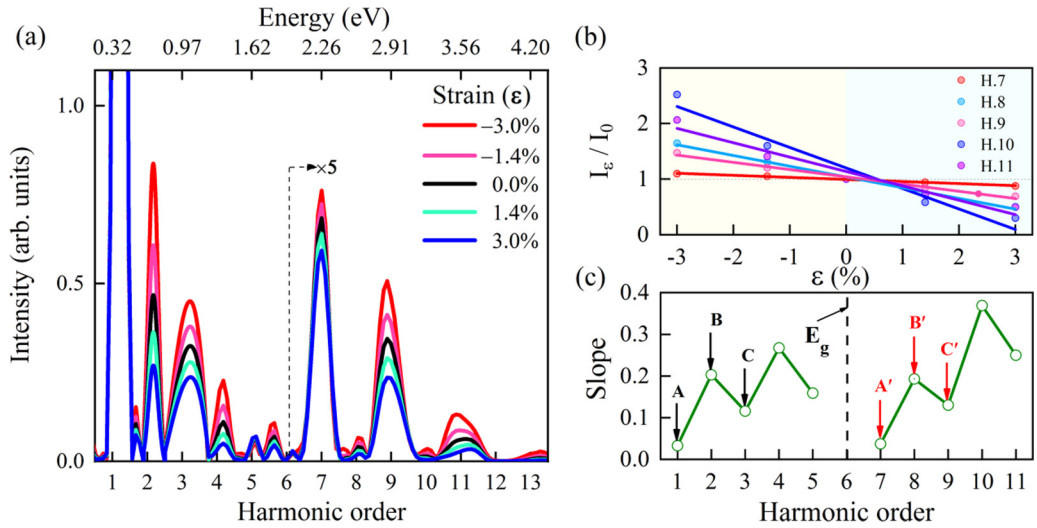

FIG. 3. Strain-dependent HHG yield for different harmonics of 1L-MoS_2. (a) Evolution of the normalized HHG spectrum under tensile and compressive strain. (b) The relative change in HHG intensity as a function of strain for representative harmonics (colored dots) and the linear fit (solid lines). (c) Applying the same method to all harmonics, the absolute value of the slope changes nearly periodically. Black and red arrows labeled as X and X' ($X = A, B, \ldots$) denote the harmonics in the first and second cycle.

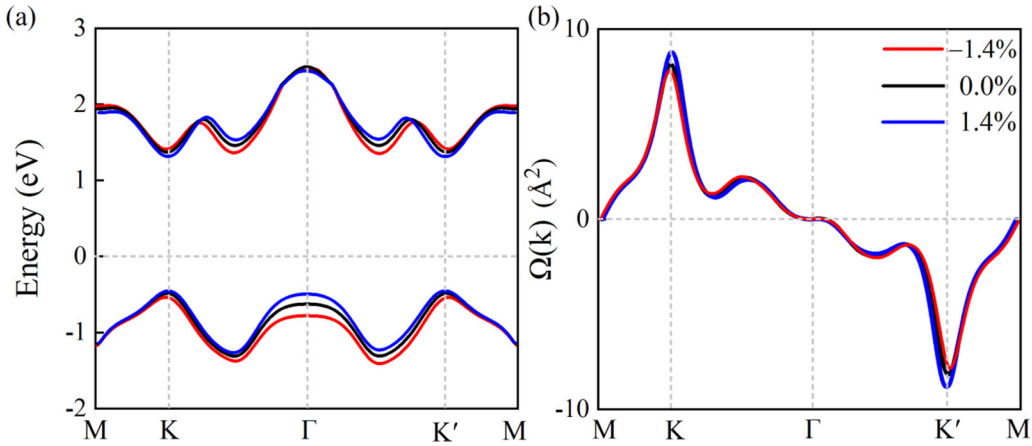

FIG. 4. (a) Evolution of band structure and (b) Berry curvature under three strain conditions, while the color of red, black, and blue represent strain of −1.4%, 0%, and 1.4%, respectively.

To uncover the underlying mechanism, we first start our discussion assuming that the semiclassical model (i.e., adiabatic evolution) is valid. Considering crystal symmetry restrictions, we expect that the emergence of even harmonics arises from materials' Berry curvature, while the odd harmonics exhibit a significant dependence on band dispersion [1,7]. In this scenario, both terms will change with uniaxial strain (Fig. 4). For a more quantitative analysis, based on symmetry features in momentum space, Berry curvature and band dispersion can be represented by a series of spatial harmonics along the K-Γ-K' direction:

$$\Omega(k) = \sum_{n=0}^{n_{\max}} \Omega_n \sin(nkd), \tag{4}$$

$$\varepsilon(k) = \sum_{n=0}^{n_{\max}} \varepsilon_n \cos(nkd). \tag{5}$$

Here, d is the lattice constant, Ω_n and ε_n are the nth Fourier coefficient of the Berry curvature and the lowest conduction band, respectively. In this semiclassical treatment, the dynamic evolution of the preexisting wave packet and the subsequently HHG emission are closely related to the magnitudes of Ω_n and ε_n [2,15].

Figures 5(a) and 5(b) show the dependence of Ω_n and ε_n on strain. The standard deviation (σ) is used to quantify the amplitude of variation for two sets of data. A smaller σ implies that the data points are closer to the mean of each set, making them decay faster as n increases (Fig. S4). Considering that the wave-packet acceleration starts from the K and K' valleys of reciprocal space, the energy dispersion near K and K' should play the most crucial role in HHG emission and can be represented by the odd-order spatial harmonics (Fig. S5). The decrease in the magnitude of σ_Ω and odd-order subset σ_ε [brighter dots in Fig. 5(b)] under compressive strain suggests that flatter band dispersion and Berry curvature may help increase intraband contributions, leading to enhanced harmonic emission.

We emphasize that although the intuitive model using pure intraband dynamics can qualitatively capture the main features of HHG, it must be scrutinized when interband transitions also contribute to the generation process. For instance, in 1L-MoS_2, the role of Berry curvature in the intraband mechanism is to introduce an anomalous in-plane current that is perpendicular to the direction of the electric field of pump laser ($J \propto \dot{k} \times \Omega \propto E \times \Omega$), giving rise to only *perpendicular* component of even harmonics. Nevertheless, the oversimplified model fails to explain the experimental observation of even harmonics polarized *parallel* to the driving field [also see Fig. 6(a)], indicating that interband dynamics is indispensable.

For the interband process, the electron-hole pair is generated, then accelerated by the laser field, and subsequently recombines coherently, emitting harmonic photons. Therein, electrons populated into the conduction bands $\Delta n_e(t)$ will oscillate in the momentum space, constituting Bloch oscillations together with intraband transitions. The value of $\Delta n_e(t)$ also oscillates in time. Therefore, accurate physical interpretation of HHG needs to consider both interband and intraband transitions.

In order to investigate the role of interband process, we compute the momentum-resolved dynamics of excited electrons in conduction bands (CBs). Firstly, we have monitored the time evolution of the number of excited electrons by projecting the time-evolved wave functions ($|\psi_{n,\mathbf{k}}(t)\rangle$) on the basis of the ground-state wave functions ($|\varphi_{n',\mathbf{k}}\rangle$),

$$\Delta n_e(t) = \frac{1}{N_{\boldsymbol{k}}} \sum_{n,n'}^{\mathrm{CB}} \sum_{\boldsymbol{k}}^{\mathrm{BZ}} |\langle \psi_{n,\boldsymbol{k}}(t) | \varphi_{n',\boldsymbol{k}} \rangle|^2, \tag{6}$$

where $N_{\mathbf{k}}$ is the total number of the $\boldsymbol{k}$ point used to sample the Brillouin zone (BZ). All conduction-band electrons are summed up and n, n' are band indices. Figure 5(c) shows that more electrons are excited with lattice contraction during each half cycle, and then most of them return to ground state. The results indicate that under compressive strain, more carriers have been promoted to higher energy levels (interband) and to a broader momentum space (intraband), jointly contributing to harmonic generation.

The higher density of excited carriers by interband transitions would further flatten out the band dispersion and Berry curvature, thus increase the intraband contributions and lead

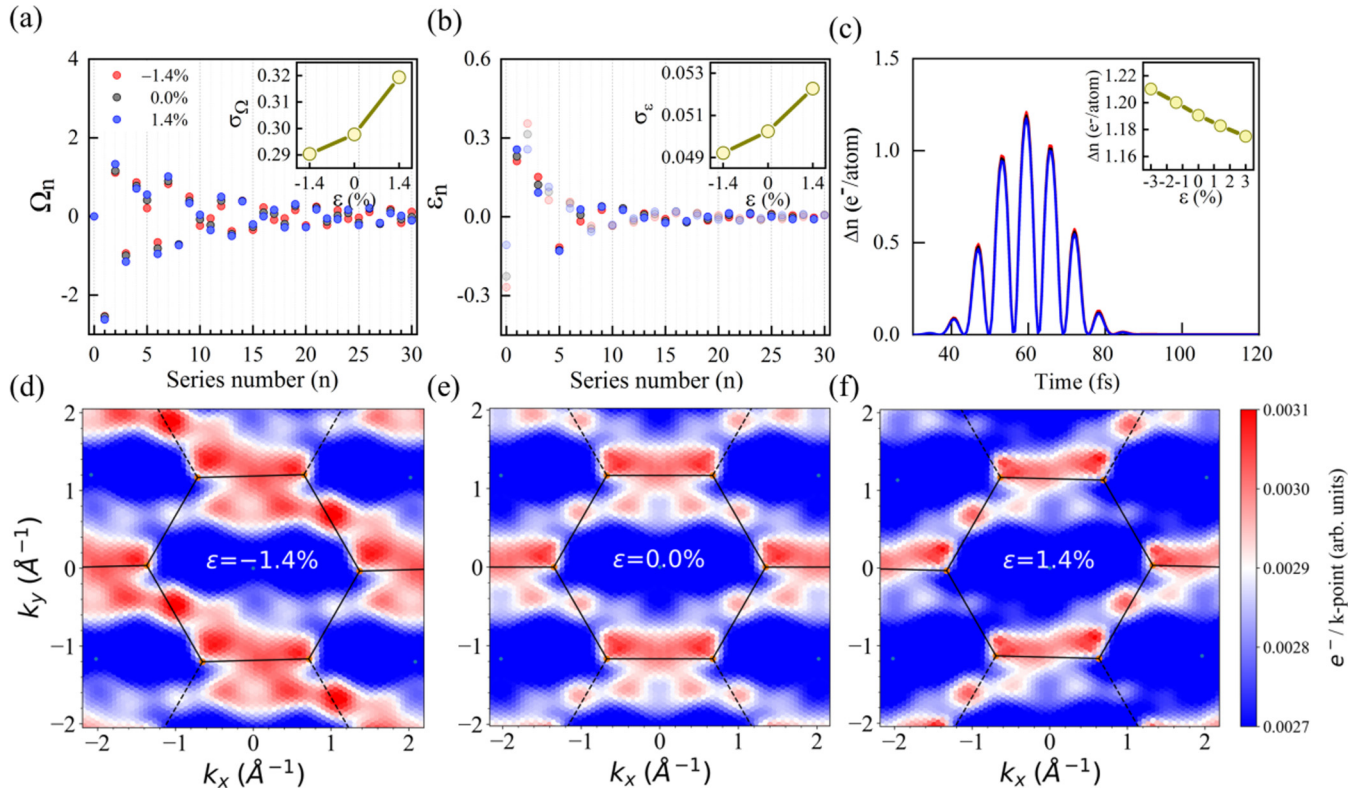

FIG. 5. Theoretical understanding of the strain modulation effect on HHG. (a), (b) Fourier series coefficients of Berry curvature and the lowest conduction-band dispersion with strain of −1.4, 0 and 1.4%. Standard deviations of data points are displayed in the inset. (c) Number of electrons excited to the conduction bands during the laser pulse. The inset shows the maximum value of excited electrons ($t = 60$ fs) as a function of strain. (d)–(f) False color representation of the momentum space-resolved distribution of the excited electrons at $t = 60$ fs under strain −1.4% (d), 0.0% (e), and 1.4% (f), respectively. The area bounded by black lines in each panel indicates the Brillouin zone.

to a cooperative effect between them. The compressive strain will smooth band dispersion and Berry curvature distributions, therefore enhances intraband processes as well as interband excitations. As a result, strain introduces cooperative intraband and interband evolutions in the HHG emission of 1L-MoS_2 via modulating the smoothness of band dispersion and Berry curvature. We note that even though the accurate assignments of interband and intraband currents might be gauge dependent [59,60], the evolution of the relative contributions of the two dynamics with respect to strain is consistent in

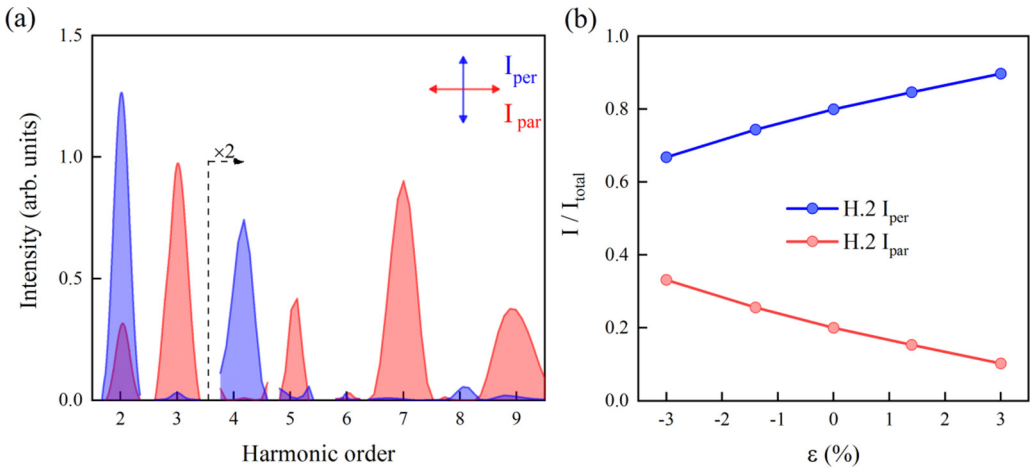

FIG. 6. Evolution of interband and intraband contributions to HHG with applied strain. (a) Computed harmonic yield from unstrained 1L-MoS_2 in the polarization basis perpendicular (blue) and parallel (red) to the linearly polarized excitation. (b) The perpendicular (I_{per}) and parallel (I_{par}) configurations of the second-order harmonic (H.2) as a function of strain. Herein, the total intensity (I_{total}) of H.2 is normalized to be 1 for all strain conditions and $I_{total} = I_{per} + I_{par}$.

different gauges [55]. The above analysis serves only as a qualitative guide for comparison.

To verify our interpretation, momentum space-resolved electron population is carried out at $t = 60$ fs, i.e., $\Delta n_e(\boldsymbol{k}) = \frac{1}{N_{\boldsymbol{k}}} \sum_{n,n'}^{\mathrm{CB}} |\langle \psi_{n,\boldsymbol{k}}(t = 60 \text{ fs})|\varphi_{n',\boldsymbol{k}}\rangle|^2$. As shown in Figs. 5(d)–5(f), it is clear that most of electrons are excited to the K and K' valleys of the BZ of 1L-MoS_2, confirming our preceding assumption. Under compressive strain, electrons traverse a lager fraction of the BZ and the number of excited electrons at each momentum $(\boldsymbol{k}_x, \boldsymbol{k}_y)$ increases simultaneously, which is direct evidence that interband and intraband dynamics cooperatively enhance the harmonics yield. The results are reversed when tensile strain is applied.

To identify the relevant contributions of intraband and interband processes to the harmonic generation, we analyze polarization-dependent components of harmonics radiation, parallel and perpendicular to the linearly polarized fundamental field, as a function of strain [Figs. 6(a) and 6(b)]. As stated above, we can make a simple correspondence between intraband (interband) transitions and the perpendicular (parallel) component of even harmonics. Besides the obvious dominance of the intraband contribution ($\frac{I_{\mathrm{intra}}}{I_{\mathrm{total}}} > 65\%$), compressive strain enhances the proportion of interband contributions and the total HHG yield.

Therefore, the explicit roles of interband and intraband dynamics in the HHG radiation are identified unambiguously. Each harmonic is produced predominated by the intraband current, while interband contribution is essential in enhancing absolute HHG yield in the entire spectrum. The calculations show that the yields from both intraband and interband transitions increase, and the proportion of the interband contribution is simultaneously enhanced when external compressive strain is applied. Our results underpin the possibility to control the HHG generation process by band engineering via mechanical means, doping, or layer stacking. This conclusion is not limited to 1L-MoS_2, and applies to other TMD materials.

Apart from the above results, another interesting phenomenon captured from Fig. 3(c) is that the slopes exhibit a periodical variation. Moreover, the repeating energy interval corresponds exactly to the band gap of the equilibrium structure. For instance, the first order has the same slope as the seventh. Even if we change the photon energy of the laser pulse, this phenomenon still prevails (Fig. S6). Consequently, one could extract both the band gap and band dispersion (encoded in estimated effective mass of electrons) from the evolution of HHG in strained samples (Fig. S7).

This observation has recovered the known wisdom that interband dynamics plays a vital role in bridging below-band-gap and above-band-gap harmonics [18,23]. Beyond that, the result implies the potential to retrieve electronic information of the solid target, such as the intrinsic band gap, i.e., the band gap that does not account for the excitonic effect, by monitoring the strain-dependent HHG yield with a high confidence level. In Ref. [11], Vampa *et al.* reconstructed momentum-dependent band gap of ZnO along the Γ-M direction by perturbing high-harmonic generation with a weak second-harmonic field. An external strain or additional field can both serve as a perturbative means. The advantage of the present approach is that the accuracy does not depend on the *a priori* functional form of the trial band structure.

IV. CONCLUSION

In conclusion, we predict that tailoring crystal structure via strain provides an effective tool to control HHG and helps clarifying the microscopic mechanism of HHG in solids. The HHG yield can be efficiently enhanced by applying compressive strain in 1L-MoS_2, beaconing a strong cooperative effect between intraband and interband contributions. Meanwhile, the relative contributions of the two dynamics are identified, i.e., intraband dynamics acts as the dominant factor of the HHG spectrum morphology, whereas interband dynamics is indispensable in modulating the absolute HHG emission. In addition, our results suggest the possibility to recover band structure based on solid-state HHG, where the intrinsic band gap is retrieved by monitoring the evolution in amplitude of HHG spectra. This work establishes a direct link between the HHG emission and underlying electronic dynamics, which would help design materials for tunable harmonic generation.

ACKNOWLEDGMENTS

We acknowledge partial financial support from the National Key Research and Development Program of China (Grants No. 2016YFA0300902 and No. 2015CB921001), National Natural Science Foundation of China (Grants No. 91850120 and No. 11774396), and "Strategic Priority Research Program (B)" of Chinese Academy of Sciences (Grant No. XDB07030100). M.-X.G. thanks S. Jiang for helpful discussions.

M.-X.G. and C.L. contributed equally to this work.

[1] S. Ghimire, A. D. DiChiara, E. Sistrunk, P. Agostini, L. F. DiMauro, and D. A. Reis, Nat. Phys. **7**, 138 (2011).

[2] T. T. Luu, M. Garg, S. Y. Kruchinin, A. Moulet, M. T. Hassan, and E. Goulielmakis, Nature (London) **521**, 498 (2015).

[3] Y. S. You, D. A. Reis, and S. Ghimire, Nat. Phys. **13**, 345 (2016).

[4] S. Han, H. Kim, Y. W. Kim, Y. J. Kim, S. Kim, I. Y. Park, and S. W. Kim, Nat. Commun. **7**, 13105 (2016).

[5] M. Sivis, M. Taucer, G. Vampa, K. Johnston, A. Staudte, A. Y. Naumov, D. Villeneuve, C. Ropers, and P. Corkum, Science **357**, 303 (2017).

[6] G. Ndabashimiye, S. Ghimire, M. Wu, D. A. Browne, K. J. Schafer, M. B. Gaarde, and D. A. Reis, Nature (London) **534**, 520 (2016).

[7] H. Liu, Y. Li, Y. S. You, S. Ghimire, T. F. Heinz, and D. A. Reis, Nat. Phys. **13**, 262 (2016).

[8] N. Yoshikawa, T. Tamaya, and K. Tanaka, Science **356**, 736 (2017).

[9] M. Garg, M. Zhan, T. T. Luu, H. Lakhotia, T. Klostermann, A. Guggenmos, and E. Goulielmakis, Nature (London) **538**, 359 (2016).

[10] F. Krausz and M. I. Stockman, Nat. Photonics **8**, 205 (2014).

[11] G. Vampa, T. J. Hammond, N. Thiré, B. E. Schmidt, F. Légaré, C. R. McDonald, T. Brabec, D. D. Klug, and P. B. Corkum, Phys. Rev. Lett. **115**, 193603 (2015).

[12] A. Lanin, E. Stepanov, A. Fedotov, and A. Zheltikov, Optica **4**, 516 (2017).

[13] M. Hohenleutner, F. Langer, O. Schubert, M. Knorr, U. Huttner, S. W. Koch, M. Kira, and R. Huber, Nature (London) **523**, 572 (2015).

[14] O. D. Mücke, Phys. Rev. B **84**, 081202(R) (2011).

[15] T. T. Luu and H. J. Wörner, Nat. Commun. **9**, 916 (2018).

[16] C. Yu, S. Jiang, and R. Lu, Adv. Phys.: X **4**, 1562982 (2019).

[17] J. L. Krause, K. J. Schafer, and K. C. Kulander, Phys. Rev. Lett. **68**, 3535 (1992).

[18] P. B. Corkum, Phys. Rev. Lett. **71**, 1994 (1993).

[19] N. Tancogne-Dejean, O. D. Mucke, F. X. Kartner, and A. Rubio, Phys. Rev. Lett. **118**, 087403 (2017).

[20] T. Otobe, Phys. Rev. B **94**, 235152 (2016).

[21] T. Tamaya, A. Ishikawa, T. Ogawa, and K. Tanaka, Phys. Rev. Lett. **116**, 016601 (2016).

[22] O. Schubert, M. Hohenleutner, F. Langer, B. Urbanek, C. Lange, U. Huttner, D. Golde, T. Meier, M. Kira, and S. W. Koch, Nat. Photonics **8**, 119 (2014).

[23] T. Higuchi, M. I. Stockman, and P. Hommelhoff, Phys. Rev. Lett. **113**, 213901 (2014).

[24] G. Vampa, C. R. McDonald, G. Orlando, D. D. Klug, P. B. Corkum, and T. Brabec, Phys. Rev. Lett. **113**, 073901 (2014).

[25] D. Golde, T. Meier, and S. W. Koch, Phys. Rev. B **77**, 075330 (2008).

[26] Z. Wang, H. Park, Y. H. Lai, J. Xu, C. I. Blaga, F. Yang, P. Agostini, and L. F. DiMauro, Nat. Commun. **8**, 1686 (2017).

[27] K. Kaneshima, Y. Shinohara, K. Takeuchi, N. Ishii, K. Imasaka, T. Kaji, S. Ashihara, K. L. Ishikawa, and J. Itatani, Phys. Rev. Lett. **120**, 243903 (2018).

[28] T. Tamaya, A. Ishikawa, T. Ogawa, and K. Tanaka, Phys. Rev. B **94**, 241107(R) (2016).

[29] N. Tancogne-Dejean, O. D. Mücke, F. X. Kärtner, and A. Rubio, Nat. Commun. **8**, 745 (2017).

[30] J. D. Cox, A. Marini, and F. J. G. De Abajo, Nat. Commun. **8**, 14380 (2017).

[31] G. Vampa, B. G. Ghamsari, S. Siadat Mousavi, T. J. Hammond, A. Olivieri, E. Lisicka-Skrek, A. Y. Naumov, D. M. Villeneuve, A. Staudte, P. Berini, and P. B. Corkum, Nat. Phys. **13**, 659 (2017).

[32] N. Tancogne-Dejean and A. Rubio, Sci. Adv. **4**, eaao5207 (2018).

[33] Z. Liu, M. Amani, S. Najmaei, Q. Xu, X. Zou, W. Zhou, T. Yu, C. Qiu, A. G. Birdwell, F. J. Crowne, R. Vajtai, B. I. Yakobson, Z. Xia, M. Dubey, P. M. Ajayan, and J. Lou, Nat. Commun. **5**, 5246 (2014).

[34] A. Castellanos-Gomez, R. Roldan, E. Cappelluti, M. Buscema, F. Guinea, H. S. van der Zant, and G. A. Steele, Nano Lett. **13**, 5361 (2013).

[35] J. Liang, J. Zhang, Z. Li, H. Hong, J. Wang, Z. Zhang, X. Zhou, R. Qiao, J. Xu, P. Gao, Z. Liu, Z. Liu, Z. Sun, S. Meng, K. Liu, and D. Yu, Nano Lett. **17**, 7539 (2017).

[36] K. He, C. Poole, K. F. Mak, and J. Shan, Nano Lett. **13**, 2931 (2013).

[37] Y. Y. Hui, X. Liu, W. Jie, N. Y. Chan, J. Hao, Y.-T. Hsu, L.-J. Li, W. Guo, and S. P. Lau, ACS Nano **7**, 7126 (2013).

[38] H. J. Conley, B. Wang, J. I. Ziegler, R. F. Haglund, Jr., S. T. Pantelides, and K. I. Bolotin, Nano Lett. **13**, 3626 (2013).

[39] J. O. Island, A. Kuc, E. H. Diependaal, R. Bratschitsch, H. S. van der Zant, T. Heine, and A. Castellanos-Gomez, Nanoscale **8**, 2589 (2016).

[40] S. B. Desai, G. Seol, J. S. Kang, H. Fang, C. Battaglia, R. Kapadia, J. W. Ager, J. Guo, and A. Javey, Nano Lett. **14**, 4592 (2014).

[41] L. Dong, R. R. Namburu, T. P. O'Regan, M. Dubey, and A. M. Dongare, J. Mater. Sci. **49**, 6762 (2014).

[42] W. S. Yun, S. W. Han, S. C. Hong, I. G. Kim, and J. D. Lee, Phys. Rev. B **85**, 033305 (2012).

[43] S. Meng and E. Kaxiras, J. Chem. Phys. **129**, 054110 (2008).

[44] W. Ma, J. Zhang, L. Yan, Y. Jiao, Y. Gao, and S. Meng, Comput. Mater. Sci. **112**, 478 (2016).

[45] C. Lian, M. Guan, S. Hu, J. Zhang, and S. Meng, Adv. Theory Simul. **1**, 1800055 (2018).

[46] M. Noda, S. A. Sato, Y. Hirokawa, M. Uemoto, T. Takeuchi, S. Yamada, A. Yamada, Y. Shinohara, M. Yamaguchi, K. Iida, I. Floss, T. Otobe, K. M. Lee, K. Ishimura, T. Boku, G. F. Bertsch, K. Nobusada, and K. Yabana, Comput. Phys. Commun. **235**, 356 (2019).

[47] C. D. Pemmaraju, F. D. Vila, J. J. Kas, S. A. Sato, J. J. Rehr, K. Yabana, and D. Prendergast, Comput. Phys. Commun. **226**, 30 (2018).

[48] A. Splendiani, L. Sun, Y. Zhang, T. Li, J. Kim, C.-Y. Chim, G. Galli, and F. Wang, Nano Lett. **10**, 1271 (2010).

[49] G. Wang, X. Marie, I. Gerber, T. Amand, D. Lagarde, L. Bouet, M. Vidal, A. Balocchi, and B. Urbaszek, Phys. Rev. Lett. **114**, 097403 (2015).

[50] K. F. Mak, K. He, C. Lee, G. H. Lee, J. Hone, T. F. Heinz, and J. Shan, Nat. Mater. **12**, 207 (2013).

[51] K. He, N. Kumar, L. Zhao, Z. Wang, K. F. Mak, H. Zhao, and J. Shan, Phys. Rev. Lett. **113**, 026803 (2014).

[52] K. F. Mak, K. L. McGill, J. Park, and P. L. McEuen, Science **344**, 1489 (2014).

[53] X. Xu, W. Yao, D. Xiao, and T. F. Heinz, Nat. Phys. **10**, 343 (2014).

[54] J. Feng, X. Qian, C.-W. Huang, and J. Li, Nat. Photonics **6**, 866 (2012).

[55] See Supplemental Material at http://link.aps.org/supplemental/10.1103/PhysRevB.99.184306, for details about other discussions, which include Refs. [61–64].

[56] E. Scalise, M. Houssa, G. Pourtois, V. Afanas'ev, and A. Stesmans, Nano Res. **5**, 43 (2011).

[57] M. Ghorbani-Asl, S. Borini, A. Kuc, and T. Heine, Phys. Rev. B **87**, 235434 (2013).

[58] F. Rossi and T. Kuhn, Rev. Mod. Phys. **74**, 895 (2002).

[59] P. Földi, Phys. Rev. B **96**, 035112 (2017).

[60] G. Ernotte, T. J. Hammond, and M. Taucer, Phys. Rev. B **98**, 235202 (2018).

[61] P. C. Becker, H. L. Fragnito, C. H. Brito Cruz, R. L. Fork, J. E. Cunningham, J. E. Henry, and C. V. Shank, Phys. Rev. Lett. **61**, 1647 (1988).

[62] M. T. Portella, J. Y. Bigot, R. W. Schoenlein, J. E. Cunningham, and C. V. Shank, Appl. Phys. Lett. **60**, 2123 (1992).

[63] S. Jiang, J. Chen, H. Wei, C. Yu, R. Lu, and C. D. Lin, Phys. Rev. Lett. **120**, 253201 (2018).

[64] I. Floss, C. Lemell, G. Wachter, V. Smejkal, S. A. Sato, X.-M. Tong, K. Yabana, and J. Burgdörfer, Phys. Rev. A **97**, 011401(R) (2018).